

Cloud Properties over the North Slope of Alaska: Identifying the Prevailing Meteorological Regimes

JOHANNES MÜLMENSTÄDT, DAN LUBIN, AND LYNN M. RUSSELL

Scripps Institution of Oceanography, La Jolla, California

ANDREW M. VOGELMANN

Brookhaven National Laboratory, Upton, New York

(Manuscript received 31 October 2011, in final form 27 March 2012)

ABSTRACT

Long time series of Arctic atmospheric measurements are assembled into meteorological categories that can serve as test cases for climate model evaluation. The meteorological categories are established by applying an objective *k*-means clustering algorithm to 11 years of standard surface-meteorological observations collected from 1 January 2000 to 31 December 2010 at the North Slope of Alaska (NSA) site of the U.S. Department of Energy Atmospheric Radiation Measurement Program (ARM). Four meteorological categories emerge. These meteorological categories constitute the first classification by meteorological regime of a long time series of Arctic meteorological conditions. The synoptic-scale patterns associated with each category, which include well-known synoptic features such as the Aleutian low and Beaufort Sea high, are used to explain the conditions at the NSA site. Cloud properties, which are not used as inputs to the *k*-means clustering, are found to differ significantly between the regimes and are also well explained by the synoptic-scale influences in each regime. Since the data available at the ARM NSA site include a wealth of cloud observations, this classification is well suited for model–observation comparison studies. Each category comprises an ensemble of test cases covering a representative range in variables describing atmospheric structure, moisture content, and cloud properties. This classification is offered as a complement to standard case-study evaluation of climate model parameterizations, in which models are compared against limited realizations of the Earth–atmosphere system (e.g., from detailed aircraft measurements).

1. Introduction

In much of the Arctic, strong surface-based inversions and persistent stratiform clouds prevail (Serreze and Barry 2005; Przybylak 2003). Despite the deceptive simplicity of the atmospheric structure, Arctic stratiform clouds present long-standing challenges to our understanding of the Arctic radiation budget (Curry et al. 1996; Uttal et al. 2002). Because of the strong ice–albedo feedback, predictions of Arctic climate change are sensitive to the radiative properties of clouds (Kay and Gettelman 2009; Vavrus 2004). Mixed-phase clouds (MPC) occur in the Arctic for a large part of the year. Because the partitioning between ice and liquid water in these clouds—and hence their radiative properties—can

vary widely, their correct representation in climate models is an urgent problem.

Mixed-phase clouds are present in the Arctic over 40% of the time (Shupe et al. 2006) and are especially prevalent during spring and fall. These clouds often have long lifetimes [Shupe (2011) notes that several days' persistence is not uncommon] and complicated structures (Morrison et al. 2012). For example, single-layer clouds constituted only half of all mixed-phase cloud observations in Shupe et al. (2006). These clouds are important for the regional heat budget, and current models have difficulty reproducing them. In particular, liquid water is present in clouds as cold as -40°C (Shupe 2011, and references therein), and modeled liquid water content at cold temperatures is often incorrect, which is a deficiency that can potentially be addressed only by the most current and sophisticated microphysics schemes. Depending on the details of the clouds, models can either overpredict or underpredict the ice- and

Corresponding author address: Lynn M. Russell, Scripps Institution of Oceanography, 9500 Gilman Dr. MC 0221, La Jolla, CA 92093.
E-mail: lmrussell@ucsd.edu

liquid-water mass mixing ratios, yielding large scatter between models and error on the order of tens of watts per meter squared on downwelling longwave radiation (e.g., Briegleb and Bromwich 1998; Curry et al. 2000; Inoue et al. 2006; Sandvik et al. 2007; Klein et al. 2009).

Correct parameterization of ice microphysics, hence, is crucial to model success in Arctic clouds. In recent years, multimoment microphysics models have become available. These models are prognostic in both particle number and mixing ratio (two “moments” of the particle size distribution) for several hydrometeor species (e.g., Fowler et al. 1996; Meyers et al. 1997; Rotstajn et al. 2000; Thompson et al. 2004, 2008; Morrison and Pinto 2005; Milbrandt and Yau 2005; Morrison and Gettelman 2008). It is generally observed [e.g., in the model intercomparisons performed by Klein et al. (2009) and Morrison et al. (2009)] that the multimoment models lead to better agreement with observations than single-moment models under the same conditions. Nevertheless, large discrepancies between model results and observations are still common. While Klein et al. (2009) find generally good agreement for ice water path (IWP) and note a factor of 3 *underestimate* of liquid water path (LWP) in single-layer MPC, Morrison et al. (2009) report that the same models *overestimate* LWP and strongly underestimate IWP in multilayer MPC only a few days earlier. Many model-sensitivity studies (e.g., Morrison and Grabowski 2008; Solomon et al. 2009; Fridlind et al. 2007) find evidence that, despite the vast progress made in the recent past, the process of further refinements is far from complete, especially in the treatment of ice-formation microphysics.

Multiple field campaigns have been carried out in the Arctic specifically to furnish observations for model evaluation. These include the Surface Heat Budget of the Arctic (SHEBA; Uttal et al. 2002) program, the Mixed-Phase Arctic Cloud Experiment (M-PACE; Verlinde et al. 2007), and the Indirect and Semi-Direct Aerosol Campaign (ISDAC; McFarquhar et al. 2011). These campaigns are instrumentation-intensive, since substantial information about clouds needs to be gathered to infer microphysical information and thence diagnose model performance. Measurements usually include size distributions and mixing ratios of liquid and various ice hydrometeor species (ideally as vertical profiles), aerosol properties, and radiative fluxes. However, field campaigns are of limited duration, and thus they cover only a limited subset of the meteorological conditions encountered in the Arctic. Even when models are found to agree well with observation, it is not clear whether that finding holds under other, unobserved conditions. When models and observations disagree, there is only limited information on what causes the disagreement.

Field campaigns are not the only source of cloud-property observations. The U.S. Department of Energy (DOE) Atmospheric Radiation Measurement Program (ARM; Ackerman and Stokes 2003) placed a site in Barrow on the North Slope of Alaska (NSA) specifically to address the shortage of cloud observations in the Arctic (Stamnes et al. 1995; Curry et al. 1996; Stamnes et al. 1999). As a result, there are now over a decade of near-continuous observations available that include a wealth of cloud-property measurements, including information on ice and liquid water content, that are potentially of great relevance to the cloud-modeling difficulties described above. However, the full time series of these observations has not been used in modeling studies thus far. The reason is that the measurements simply extend over too much meteorological phase space and need to be reduced to a manageable number of test cases before they can be used effectively. What is needed is a classification of the available data into categories of similar atmospheric states. One way this classification can be achieved is to identify synoptic-scale and mesoscale meteorological regimes that produce distinct cloud states at the cloud-observing site.

Despite the climatic importance of the pervasive stratiform cloud cover in the high Arctic, discussion in current literature of the relationship between prevailing Arctic meteorology and cloud properties is incomplete. Patterns of cyclones and anticyclones have been discussed for many years, including frequent anticyclones in the Beaufort Sea region (Reed and Kunkel 1960). Stone (1997) demonstrates that Barrow is a representative site for investigating climate change impacts on cloud cover for the western Arctic, as it alternates between influences of cyclonic activity originating in the North Pacific and anticyclones in the Beaufort Sea. Serreze et al. (1993) describe the seasonality of Arctic synoptic activity. Cyclonic activity in winter tends to be localized to the eastern Arctic more than the Barrow region. Winter anticyclones, on the other hand, prevail over eastern Siberia, the central Arctic Ocean, and over the Alaska/Yukon region, and all of these regions can directly influence conditions at Barrow. During summer, the East Siberian Sea and Beaufort Sea regions often replace Siberia and Alaska/Yukon as centers of anticyclonic activity. Cyclonic activity during summer tends to arrive at Barrow from southerly directions, such as the Chukchi Sea. Cyclonic activity north of 65°N increases between April and June, leading to a dramatic increase in the frequency of stratiform cloud cover and reduction in the frequency of surface-based temperature inversions, and it also corresponds with the onset of snow and sea ice melt. Overland (2009) describes the seasonal evolution of climatological anticyclonic activity in the

western Arctic Ocean. During winter, high sea level pressure frequently ranges from Siberia to Alaska and Canada, spanning the entire Beaufort Sea. A more localized Beaufort Sea high tends to occur in spring and autumn. Maxwell (1981) characterizes the eastern Beaufort Sea region as alternating between cyclonic and anticyclonic activity, whereas all other sectors of the Canadian Arctic islands are dominated either by cyclones or anticyclones.

The relationship between prevailing Arctic meteorological regimes and sea ice dynamics has been discussed by several authors (Rogers 1978; Parkinson 1990; Proshutinsky and Johnson 1997; Barber and Hanesiak 2004). There is much less discussion in the literature that quantitatively relates Arctic meteorological regimes to cloud amount and cloud properties. Reports of atmospheric field campaigns discuss the synoptic conditions pertaining to specific experimental case studies in a climatological context (e.g., Curry et al. 2000; McFarquhar et al. 2011), but most studies of Arctic cloud cover fall into one of two categories: 1) quantifying annual cycles and multidecadal trends in cloud amount and cloud properties (e.g., Curry and Ebert 1992; Curry et al. 1996; Shupe and Intrieri 2004; Wang and Key 2003, 2005) or 2) cloud formation and persistence as a response to general meteorological characteristics, such as advection of air masses over surfaces of contrasting temperature, and presence of sea ice leads (e.g., Jayaweera 1982; Tsay and Jayaweera 1984; Curry and Herman 1985; Kay and Gettelman 2009). In these various studies, discussion of meteorological regime influences on cloud cover tends to be mainly qualitative. The contribution of the present study to climatological understanding of the high Arctic is to identify the prevailing meteorological regimes influencing the western Arctic as observed at Barrow, and at the same time to show their influence on observed cloud properties.

In the next section we perform a classification of the meteorology at the Barrow ARM site using 11 years of surface meteorological observations. The relationship of this classification to the synoptic-scale meteorological influences on Barrow is discussed in section 3. Section 4 investigates the properties of clouds and radiative fields in the different categories and finds significant differences between the categories. We describe how the method can be used to produce test cases for model evaluation in section 5 and conclude with a summary of the main findings in section 6.

2. Classification method

Objective classification algorithms have been used previously (e.g., Jakob and Tselioudis 2003; Gordon

et al. 2005; Marchand et al. 2009) to find meteorologically significant patterns in atmospheric observations. Those authors used a large number of input variables (vertical profiles of clouds, satellite cloud scenes, and synoptic fields) to derive categories of cloud cover on synoptic scales. This work is the first to identify Arctic meteorological regimes by clustering techniques. Our classification is intended to study cloud observations at one specific location (the ARM NSA site), and, owing to the sparseness of observations in the Arctic, our work is based on local inputs, in contrast to the above references. No cloud properties are used as clustering inputs, allowing us to identify unbiased differences in cloud properties between meteorological regimes. In this section we describe the method and apply it to ARM NSA observations.

a. Description

Classification is performed by a clustering algorithm. We chose k -means clustering (MacQueen 1967; Hartigan 1975; Hartigan and Wong 1979) for its computational simplicity. The algorithm groups the input observations into clusters in the n -dimensional space formed by n clustering variables. It proceeds by an iterative agglomeration in which data points are merged into clusters so that the sum of distances squared within each cluster is minimized (in our case, the distance is the n -dimensional Euclidean distance). Each meteorological observation x_i is a point in the n -dimensional space. *Observation* for our purposes refers to a 24-h average of the selected measurements: monthly air temperature anomaly, surface pressure, monthly relative humidity anomaly, and the horizontal wind components. Temperature, pressure, and relative humidity are measured at 2-m height; wind speed is measured at 10-m height. The index i runs over the observations, in our case the 24-h-averaged values from 0000 UTC 1 January 2000 to 2359 UTC 31 December 2010. The monthly temperature (relative humidity) anomaly rather than temperature (relative humidity) is used as a clustering variable to account for the seasonal variation of temperature (relative humidity). The anomaly is calculated relative to the 11-yr mean temperature (relative humidity) for each calendar month. All input variables are scaled by their standard deviations to provide appropriate relative weights in the clustering procedure.

The number of clusters k in the solution needs to be prescribed in the k -means clustering algorithm, as do initial cluster centroids μ_0 . A variety of methods exists to determine the optimal number of clusters. The initial centroids are often chosen at random from the input data points. We follow this approach and furthermore use the stability (or instability) of the

clustering against different initial random choices as a criterion to evaluate the suitability of the solution. If the clusters obtained for a given choice of k are not stable for different initial seeds, we consider that value of k unsuitable. The space of seed choices is sampled by rerunning the clustering 10 000 times with randomly chosen data points. This stability criterion dramatically narrows the choice of k values; we initially considered the range $k = 3$ –12 and found that only $k = 3$ and 4 are stable. We made our final choice in favor of the $k = 4$ solution because that solution, unlike the $k = 3$ solution, leads to a clear correspondence between clusters and the manual synoptic classification described below.

Several further tests were conducted to test the stability of the clustering solution. Instead of clustering the entire 11 years of observations, subranges were chosen and found to yield a similar four-cluster solution. When the surface pressure was replaced by the monthly anomaly of surface pressure, a similar four-cluster solution emerged. Finally, when the observed relative humidity anomaly was replaced with the relative humidity anomaly from the National Centers for Environmental Prediction (NCEP)–National Center for Atmospheric Research (NCAR) reanalysis (which has similar features but is more normally distributed), a similar four-cluster solution resulted.

b. Application to ARM NSA observations

Figures 1 and 2 illustrate the climatology of the NSA site. Situated at 71.3°N, 156.8°W, Barrow has mean air temperature above freezing only from June to September. Snow covers the land surface for nine months of the year. The sea ice extends to the shore in winter, usually retreating to $O(100)$ km offshore by autumn, but as much as several hundred kilometers in some years (Maslanik et al. 1996; Serreze and Barry 2005). For much of the year, and especially when the sun is near or below the horizon, there is persistent low-level stratus cloud cover. Forty percent of stratus cover is multilayered (Shupe 2011). Clouds always contain ice except during the peak summer insolation (Stamnes et al. 1999). The prevailing wind direction is northeasterly with several hundred kilometers or greater fetch over the Beaufort Sea and Arctic Ocean.

Distributions of the surface observations in each cluster are shown in Figs. 3 and 4. Their properties (represented by the location of the 25th–75th percentile of the distribution for the box-and-whiskers plot, and by the maximum for the wind rose plots) are summarized in Table 1. Each cluster has a combination of surface-meteorological properties that is clearly distinct from all other clusters.

Frequency distributions are shown in Fig. 5. These distributions show the number of days for which the surface conditions are associated with each cluster. The cluster with the highest surface-pressure observations occurs most frequently in winter and least frequently in summer, consistent with the seasonal variation reported by Serreze et al. (1993).

The properties of the clusters described above indicate that the clustering method carves out different regions in the distribution of each input variable in a way that results in meteorologically coherent phase-space regions that account for the multivariate correlations. This means that each cluster picks features in a subset of the variables and groups them together in a way that differs from all other clusters, as summarized in Table 1. Consequences of synoptic-scale meteorology and cloud properties will be established in the following sections. Finally, we note that no single variable or linear combination of variables (e.g., as from principal components analysis) explains a large fraction of the variance in the data, and thus in one- or two-dimensional projections of the measurements no clustering is apparent.

3. Synoptic-scale influences on Barrow and their relation to the meteorological categories

The climatology of Barrow was described in section 2b. We now describe a manual classification of two representative years (2000 and 2009) of the NCEP–NCAR reanalysis 1 (Kalnay et al. 1996) to identify synoptic regimes. Since the local meteorology at Barrow is influenced by synoptic-scale features, we expect the two classification systems to be correlated. The synoptic classification—which incorporates assimilated observations uncorrelated with the observations at Barrow—can therefore serve as a test dataset to evaluate the local classification.

Przybylak (2003) and Serreze and Barry (2005) describe the Pacific region as a “transition region,” lying in proximity to two strongly contrasting and well-developed air pressure systems, the Aleutian low and the Siberian high. The Siberian high is driven mainly by radiative cooling, and its cold air mass is constrained largely by topography. It is strongest during winter, exists during autumn and spring, and in summer is often replaced by mean low pressure. When it governs the weather at Barrow, there are usually weak winds and cold dry air. The Aleutian low is a complex feature persisting year-round and is weakest in summer. It is maintained in part by its position downstream of a major midtropospheric stationary trough where cyclogenesis is favored by upper-level divergence, and in part by surface heating contrasts involving the relatively warm ocean adjacent to the ice margin and the colder land. When the

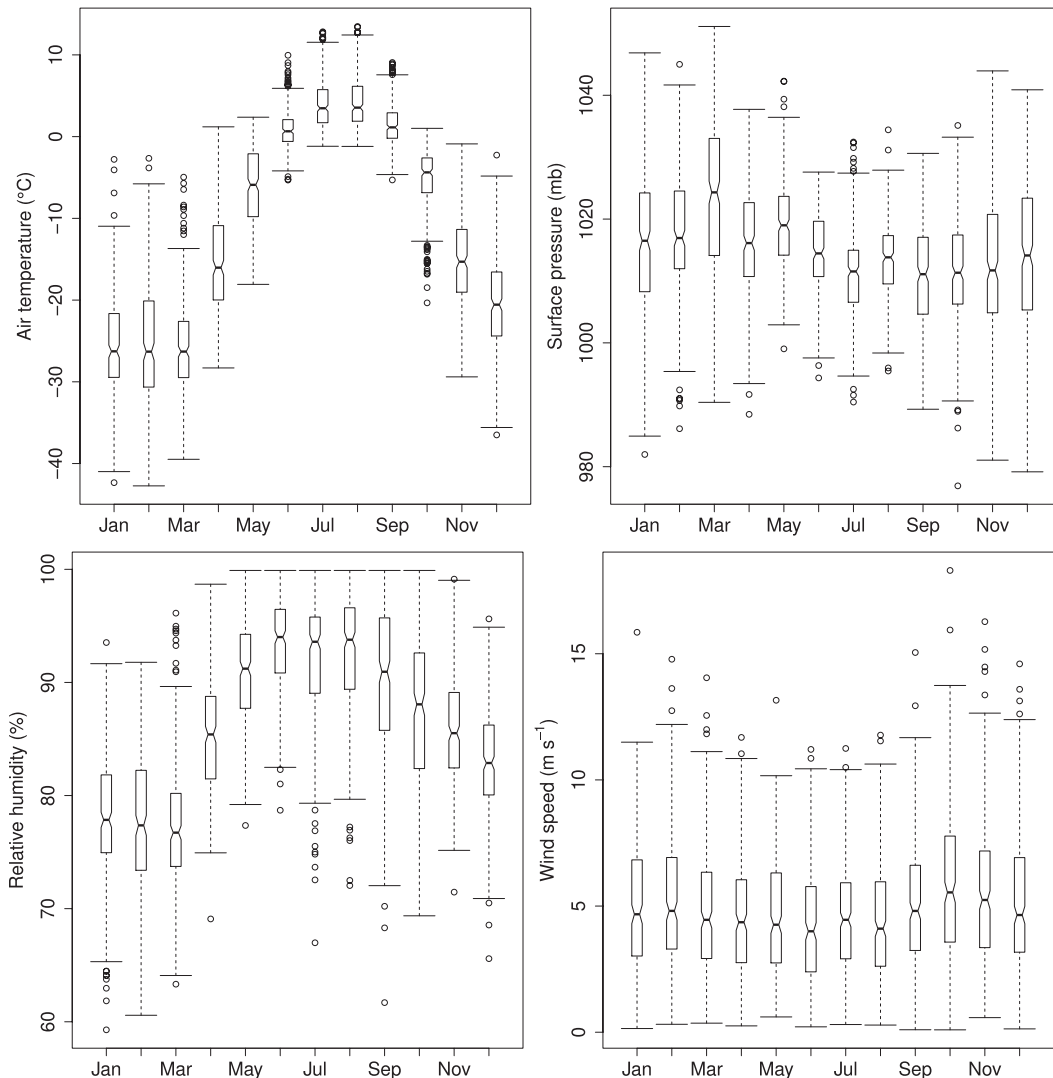


FIG. 1. Climatology of the surface observations over the 11 years used in this study. The median is indicated by the bar; the first and third quartile lie at the upper and lower edges of the box; the whiskers extend to the most extreme data point that is no more than 1.5 times the interquartile range (IQR) from the box; any data points extending beyond 1.5 IQR beyond the box are indicated by dots. The notch extends to $\pm 1.58 \text{ IQR} / \sqrt{n}$ (where n is the number of data points) and roughly indicates a 95% confidence interval on the median (McGill et al. 1978).

Aleutian low governs the weather, there are usually strong winds with warmer and moist air. Another feature of the Pacific region is a low frequency of cyclonic activity (Przybylak 2003; Serreze and Barry 2005), calculated by Serreze et al. (1993) as occurring less than 3% of the time in daily gridded sea level pressure records. The existence of zonally oriented orographic barriers—the Koryak, Chukchi, and Brooks Ranges—largely constrains cyclones to enter the region only through the narrow Bering Strait. However, this implies that cyclones that do enter the Pacific region must transport considerable warmth and moist air, resulting in a considerable increase in air temperature and precipitation.

These synoptic regimes can be readily identified in NCEP or European Centre for Medium-Range Weather Forecasts (ECMWF) reanalysis data via the synoptic and mesoscale fields of sea level pressure, winds at 850 hPa, and precipitable water vapor. To compare with our clustering results, we manually classified these synoptic regimes for two representative years. Two years were used to allow us to draw statistically significant conclusions about all identified regimes. We chose 2000 and 2009, giving consideration to any gaps in the instrumental record at Barrow. We do not expect other years to yield significantly different results. The classification used the daily average sea level pressure, 850-hPa

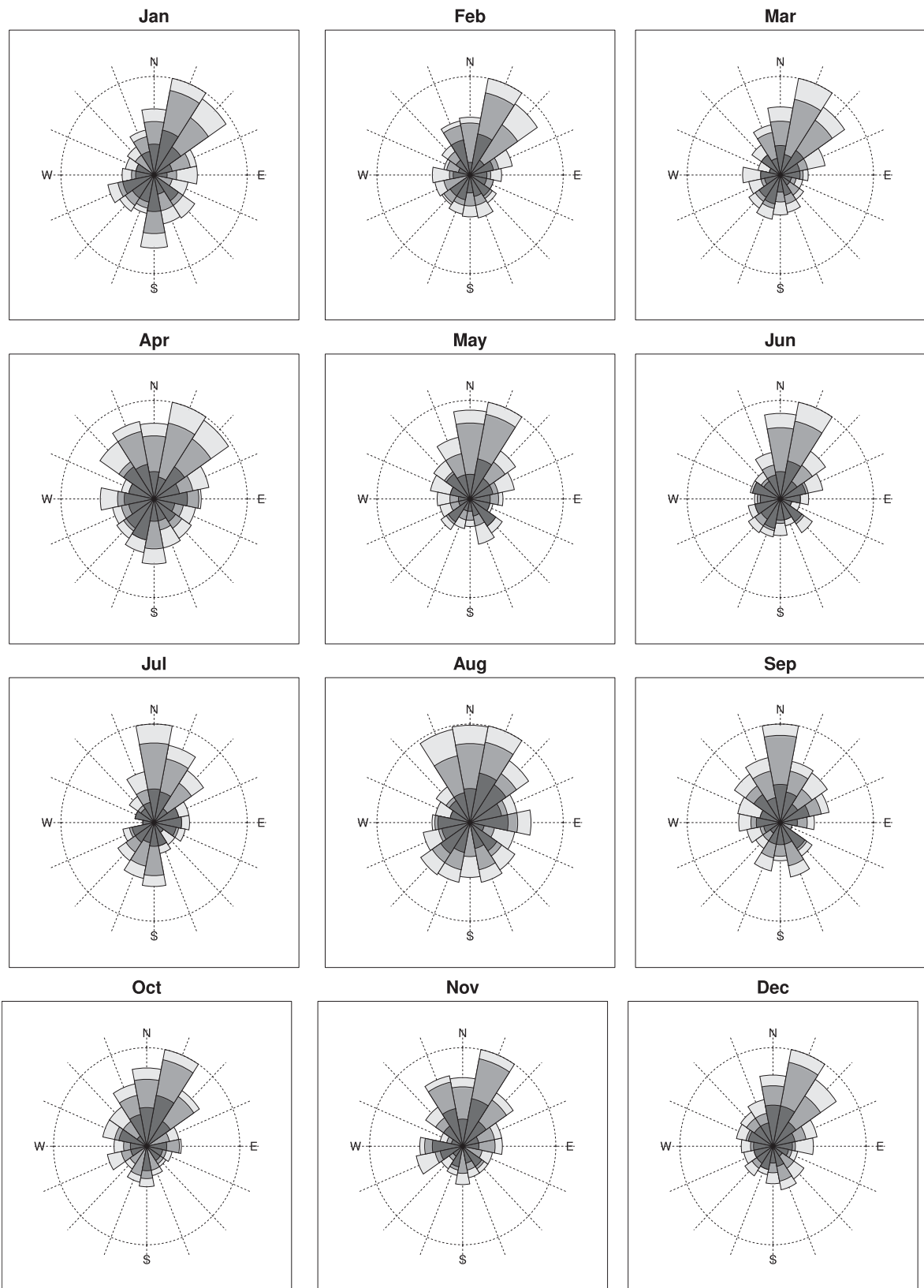


FIG. 2. Climatology of the surface wind direction over the 11 years used in this study. Wind speed is categorized as calm ($< 2.5 \text{ m s}^{-1}$; no entry); light (between 2.5 and 5 m s^{-1} ; light gray); moderate (between 5 and 10 m s^{-1} ; medium gray); and high ($> 10 \text{ m s}^{-1}$; dark gray).

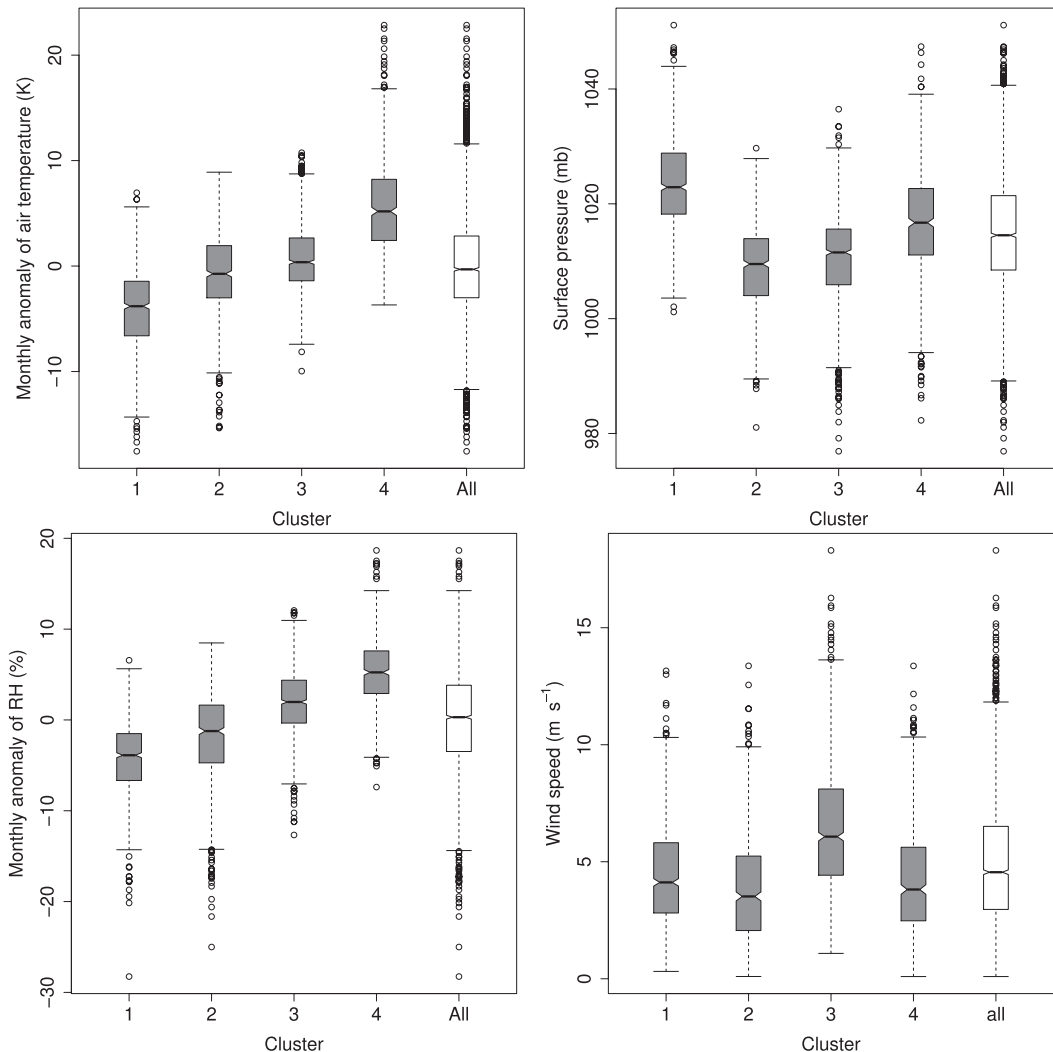


FIG. 3. Distribution resolved by cluster of air temperature anomaly, surface pressure, relative humidity anomaly, and wind speed. The median is indicated by the bar; the first and third quartiles lie at the upper and lower edges of the box; the whiskers extend to the most extreme data point that is no more than 1.5 times the IQR from the box; any data points extending beyond 1.5 IQR from the box are indicated by dots. The notch extends to $\pm 1.58 \text{ IQR} / \sqrt{n}$ (where n is the number of data points) and roughly indicates a 95% confidence interval on the median (McGill et al. 1978).

wind, and column precipitable water fields from the NCEP–NCAR reanalysis 1 (Kalnay et al. 1996), gridded to 2.5° resolution and plotted as polar stereographic contours north of 45°N latitude. For each day, the location of the synoptic system most strongly influencing Barrow was subjectively determined from the gridded fields. After identifying the location of the controlling synoptic system, a second pass was performed to group the synoptic systems according to type (high pressure or low pressure) and geographic area. If no system could be clearly discerned, the day was classified as unclassified.

Our classification of the synoptic analysis charts leads to conclusions consistent with the climatology described above. The synoptic systems governing the meteorology

at Barrow are predominantly high pressure over the Arctic Ocean or low pressure over the Aleutian and Bering Sea. The Siberian high is farther from the site, but still frequently exerts influence. Low pressure over the Beaufort Sea and Arctic Ocean also frequently controls the meteorology. Table 2 lists the frequency of occurrence for these synoptic regimes (i.e., the number of days for which Barrow is under the influence of each system).

The detailed correlation between the synoptic regimes and the clustering regimes is given in Table 3. Note that different synoptic pictures can produce similar local conditions, since these are determined in large part by advection. For this reason, synoptic categories are combined in Table 3 if they lead to similar flow regimes.

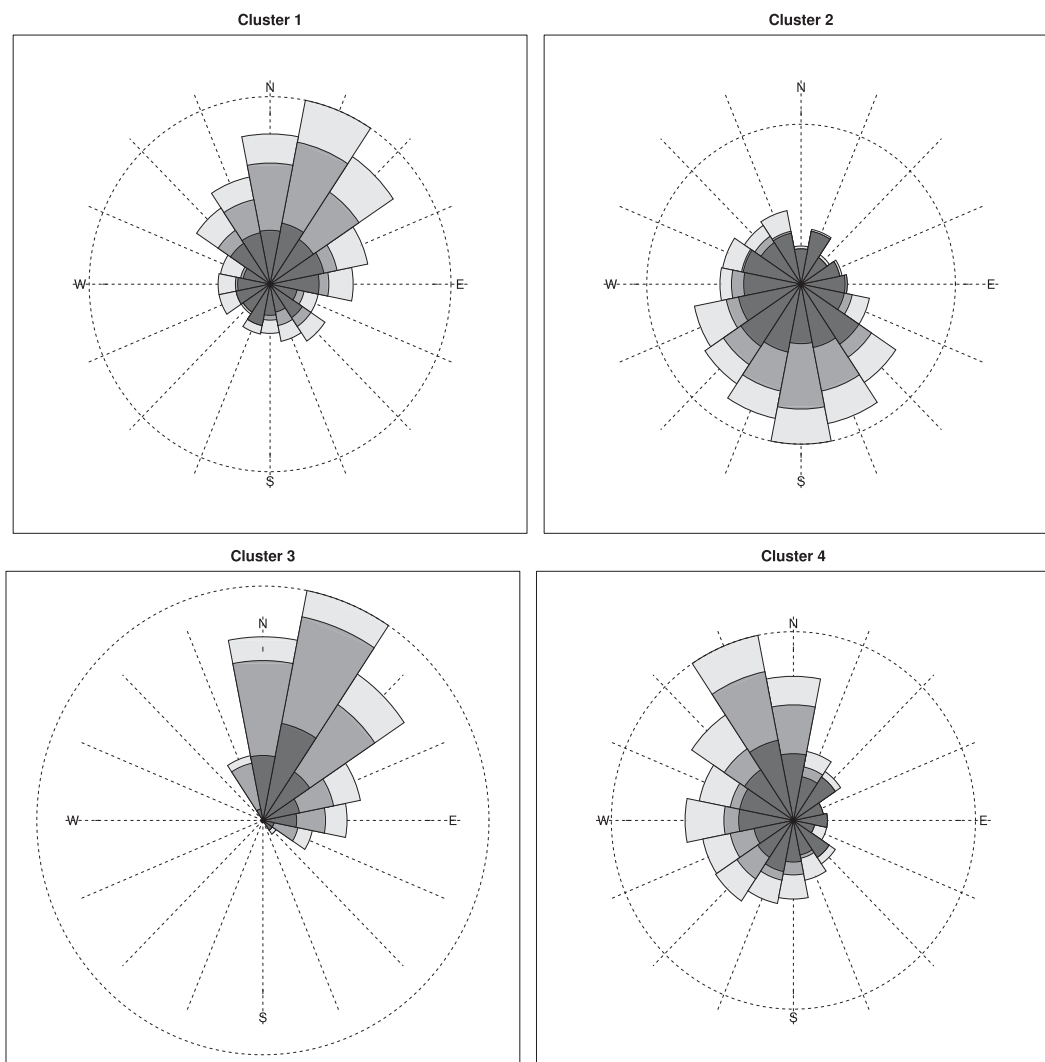


FIG. 4. Distribution resolved by cluster of the surface wind direction. Wind speed is categorized as calm ($<2.5 \text{ m s}^{-1}$; no entry); light (between 2.5 and 5 m s^{-1} ; light gray); moderate (between 5 and 10 m s^{-1} ; medium gray); and high ($>10 \text{ m s}^{-1}$; dark gray).

For example, on 45% of the days in cluster 3, Barrow was under the influence of low pressure systems to the south (over the Aleutian and Bering Seas), and on 29% of days it was under the influence of high pressure systems over the Arctic Ocean. Both the low pressure systems to the south and the high pressure systems to the north lead to strong easterly to northeasterly winds at Barrow at the surface. However, as we shall see below,

at the higher levels the flow is dominated by moist maritime air advected over the Alaskan peninsula by the low pressure systems over the Gulf of Alaska.

We now turn to composite Arctic-wide synoptic charts for each of the local meteorological categories, shown in Figs. 6–9 for the sea level pressure, air temperature (monthly anomaly), horizontal wind, and precipitable water vapor (monthly anomaly) fields, to place the local

TABLE 1. Surface-meteorology properties of each cluster.

Cluster	Frequency	Temperature anomaly	Pressure	Relative humidity anomaly	Wind speed	Wind direction
1	900	Low	High	Dry	Average	NE
2	698	Average	Low	Dry	Average	S
3	1068	Average	Low	Humid	High	NE
4	587	High	Average	Humid	Average	NW

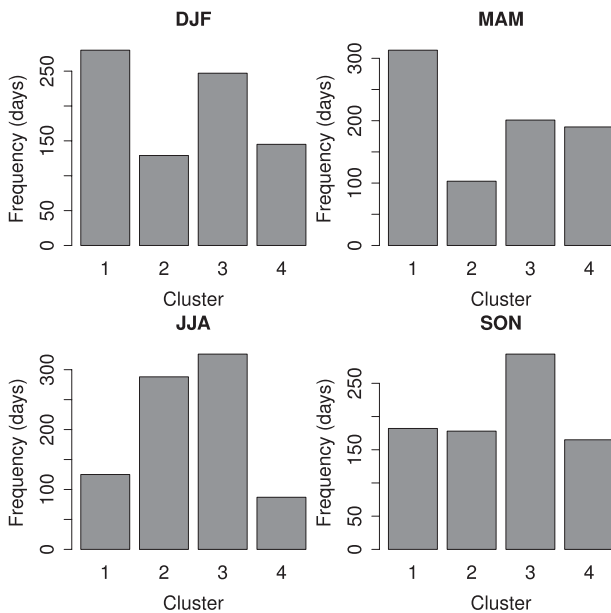


FIG. 5. Frequency of occurrence of the four categories by season.

conditions in synoptic-scale context. Cluster 1 is dominated by strong anticyclones over the Arctic Ocean, with pressure at Barrow of 1022 hPa and mean central pressure of 1025 hPa (about 8 hPa higher than the 11-yr mean strength of the Arctic Ocean high and shifted toward the Alaskan coast). The wind direction at 850 hPa shows the anticyclonic circulation, which advects air to Barrow from over the Beaufort Sea and Arctic Ocean. Since this cluster predominantly occurs while the sea ice extends to the coast, the advected air mass is anomalously cold and dry, and conditions at Barrow in this regime resemble polar desert. (We will see below that during the part of the year with open water near Barrow, cloud structures consistent with local evaporation occur.)

Cluster 2 is characterized by strong low pressure in the Arctic Ocean and Beaufort Sea, approximately 11 hPa lower than the 11-yr average, connected by a weak trough to an average-strength center of low pressure in the Gulf of Alaska. The strong low pressure systems in the Arctic Ocean advect cold and dry polar air to Barrow from over the Arctic Ocean, East Siberian Sea, and Chukchi Sea. As a result of the synoptic flow, this cluster is anomalously cold and dry even though sea level pressure at Barrow is below average.

Cluster 3 is a mixture of strong low pressure systems over the Aleutian Islands and Bering Sea, advecting moist air from the Gulf of Alaska, and weak high pressure systems over the Arctic Ocean. The sea level pressure in the Bering Sea is approximately 7 hPa lower than the climatological mean, while the pressure in the central Arctic Ocean is approximately 2 hPa higher. At

TABLE 2. Frequency of occurrence of synoptic systems controlling conditions at Barrow. Classification is based on daily-average fields of sea level pressure, 850-hPa winds, and precipitable water vapor in NCEP–NCAR reanalysis of two representative years (2000 and 2009).

Synoptic category	Absolute frequency	Relative frequency (%)
Arctic Ocean high	166	26.1
Aleutian and Bering Sea low	133	20.9
Siberian high	98	15.4
Beaufort Sea and central Arctic Ocean low	96	15.1
Siberian and Chukchi Seas low	73	11.5
Aleutian and Bering Sea high	20	3.1
Uncategorized	50	7.9

the low levels, the cyclonic flow off the Gulf of Alaska is blocked by the coastal ranges. At the higher levels, moisture is transported across the Alaskan peninsula and the Yukon and arrives at Barrow predominantly in easterly winds across the Beaufort Sea. The air arriving at Barrow is thus relatively dry at low levels even when Barrow is under cyclonic flow, but moist in the mid and upper levels. The 850-hPa wind, which is predominantly easterly at Barrow, is fast and roughly parallel to the orographic barriers, explaining the observed high surface winds in this cluster. In this and the preceding clusters, the difference in wind direction at Barrow between the 850-hPa level (shown in Fig. 9) and the surface wind (shown in Fig. 4) is consistent with geostrophic flow impeded by surface friction.

Cluster 4 is dominated by low pressure over the Aleutian and Bering Seas. Compared to the climatological average, the central pressure is only slightly depressed (1005 vs 1007 hPa in the climatological mean), but because the center of low pressure is displaced westward and the zonal extent of the trough is shortened sufficiently so that it no longer extends into the Gulf of Alaska, unimpeded advection of warm and moist Pacific air to Barrow is permitted through the Bering Strait. (In this cluster, the difference in wind direction between the surface and the 850-hPa level is larger than in the other clusters, which is explained by interference from the orographic barriers to the south of Barrow.) Thus, this is the warmest and moistest cluster (and, as we will show in the next section, has the most opaque cloud), representative of maritime Arctic conditions.

Comparing the clustering results with the synoptic classification, we can therefore identify a correspondence between each cluster and a synoptic regime that well explains the local observations in terms of synoptic-scale flow patterns. In summary, this correspondence is as follows:

TABLE 3. Correlation table between synoptic and local classification. Cell entries give the percentage of days in each cluster on which a given synoptic system was identified in a representative 2-yr time period (2000 and 2009). Columns are further grouped by location (north or south of Barrow) and type (high or low pressure) of the synoptic system. For each local category, the most common synoptic categories are identified, and the fraction of days accounted for by these categories is given in bold face. Cluster 1 corresponds to high pressure systems to the north; cluster 2 corresponds to low pressure systems to the north; cluster 3 corresponds to high pressure systems to the north and low pressure systems to the south, both causing easterly 850-hPa winds at Barrow (cf. Fig. 9); and cluster 4 corresponds to low pressure systems in the Siberian, Chukchi, and Bering Seas with predominantly southerly to westerly flow.

Cluster	Low pressure			High pressure		
	North		South	North		South
	Beaufort Sea and Central Arctic Ocean low (AOL)	Siberian and Chukchi Seas low (SL)	Aleutian and Bering Sea low (ABL)	Arctic Ocean high (AOH)	Siberian high (SH)	Aleutian and Bering Sea high (ABH)
1	5	7	11	47	26	4
	Combined: 72			Combined: 73		
2	48	24	13	1	11	2
3	7	3	45	29	16	1
			Combined: 74			
4	12	24	27	19	8	11
		Combined: 51				

cluster 1—high pressure systems to the north, with easterly to northeasterly wind directions,

cluster 2—low pressure systems to the north, with westerly winds,

cluster 3—high pressure systems to the north and low pressure systems to the south, both bringing easterly winds, and

cluster 4—low pressure systems in the Siberian, Chukchi, and Bering Seas, with predominantly southerly to westerly flow.

4. Cloud and radiation properties of the categories

We now turn to the value of the classification scheme in analyzing cloud-property categories, which is the overall aim of the method. As the design criterion of the ARM NSA site was to study cloud, the site is equipped with a large variety of cloud observation instrumentation. This includes surface-meteorology instrumentation, Total Sky Imager (TSI) cloud-cover cameras, microwave radiometers (MWRs) for liquid water path and precipitable water vapor (PWV), millimeter-wavelength cloud radar (MMCR) and lidar to determine cloud boundaries, and Sky Radiometers on Stand for Downwelling Radiation (SKYRADs) for long- and shortwave radiative fluxes. In addition, the radar and lidar measurements are combined in the Active Remote Sensing of Clouds (ARSCL) data product to determine cloud height boundaries (Clothiaux et al. 2000). Radar, lidar, and MWR are combined in the Microbase product (Zhao et al. 2012) to determine vertical profiles of liquid and ice water content

(LWC and IWC, respectively). The National Oceanic and Atmospheric Administration (NOAA) Climate Monitoring and Diagnostics Laboratory (CMDL) Aerosols Group [now the NOAA Earth System Research Laboratory (ESRL) Global Monitoring Division (GMD) Aerosols Group] provides measurements of aerosol properties at the same location (Bodhaine 1989).

Variables we have considered are cloud frequency of occurrence in the column separated by height of cloud base (clear, midlevel, and low-level), as determined by ARSCL; the TSI opaque and thin cloud sky cover; the MWR liquid water path and precipitable water vapor; the ice water path obtained by vertically integrating the Microbase IWC; the SKYRAD downwelling longwave flux; and the concentration of condensation nuclei reported by NOAA-CMDL. Since the longwave flux, liquid water path, and precipitable water vapor have strong seasonal dependencies, anomalies relative to the 11-yr monthly means are used for these variables.

Table 4 summarizes the cloud properties of each cluster. Cluster 1 is the least cloudy by all variables considered, with the highest clear-sky fraction, lowest average sky cover, lowest PWV, LWP and IWP, and lowest DLW. Clusters 2 and 4 predominantly have low cloud bases with occasional midlevel bases; cluster 3 is also dominated by low cloud, but occasionally has clear sky. PWV is lowest in cluster 1 and increases with cluster number; the median monthly PWV anomaly is negative for clusters 1 and 2, approximately 0 for cluster 3, and positive for cluster 4. The median DLW monthly anomaly is negative for cluster 1, slightly negative [within the

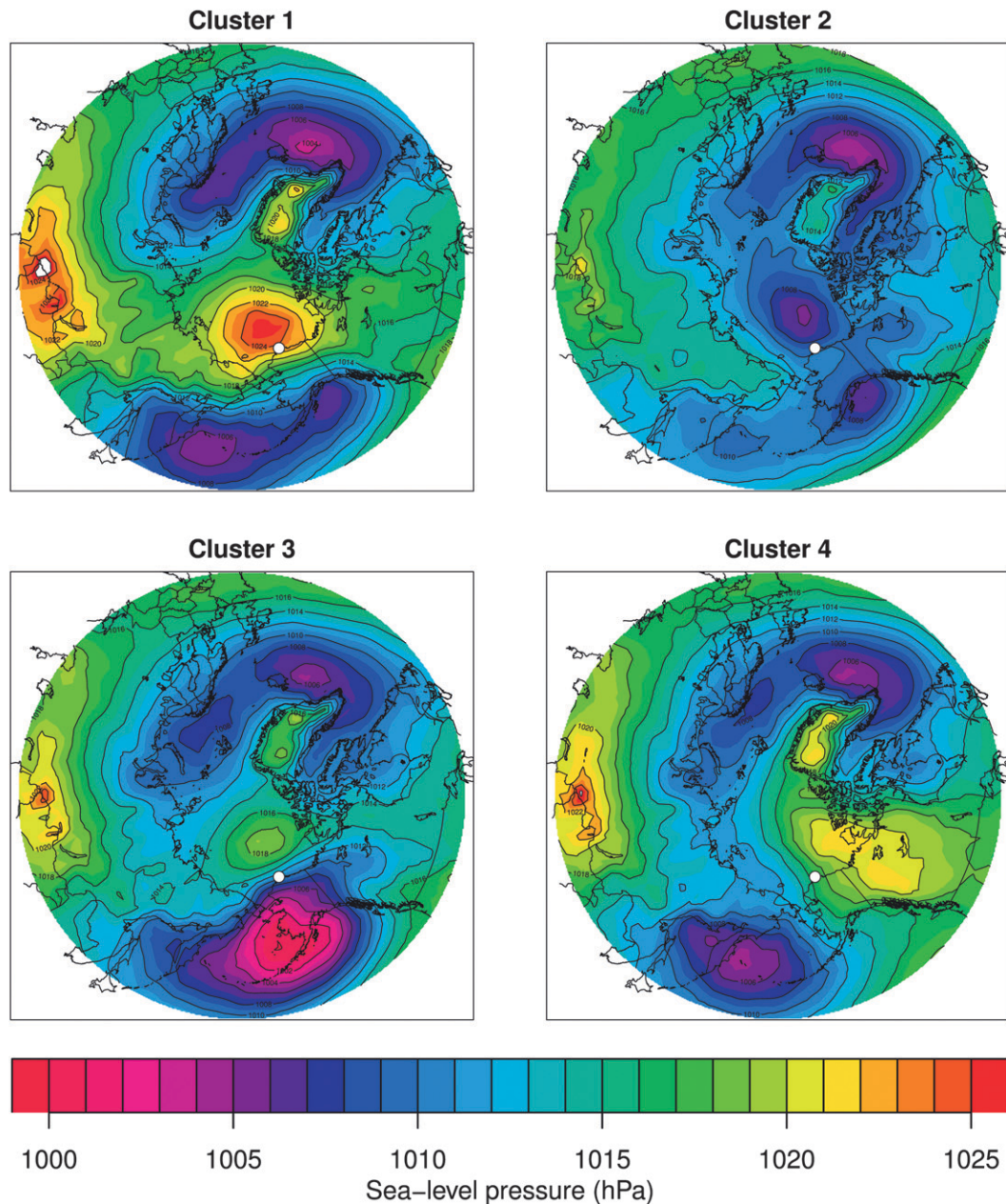


FIG. 6. NCEP-NCAR reanalysis 1 sea level pressure composites for each local meteorological category. Barrow is indicated by the white circle. Cluster 1 is dominated by high pressure over the Arctic Ocean. Low pressure over the Arctic Ocean and Beaufort Sea characterizes cluster 2. Cluster 3 is a mixture of strong low pressure systems over the Aleutian Islands and the Bering Sea and weak high pressure systems over the Arctic Ocean. In cluster 4, the usual trough over the Aleutian Sea and Gulf of Alaska is shifted toward the northwest, allowing advection of Pacific air to Barrow through the Bering Strait.

interquartile range (IQR) of 0] for cluster 2, slightly positive for cluster 3, and positive for cluster 4. CN concentrations are lowest for clusters 1 and 3 and highest for clusters 2 and 4. To the extent that local meteorological conditions can be attributed to synoptic-scale features, we can identify the origins of these cloud properties in

the synoptic characterization we provided in section 3 for each cluster. For cluster 1, we have seen that the anticyclonic flow from the Arctic Ocean explains the dry conditions that are also reflected in the cloud properties. Clusters 2 and 4 are dominated by low pressure synoptic systems, explaining the pervasive broken or overcast

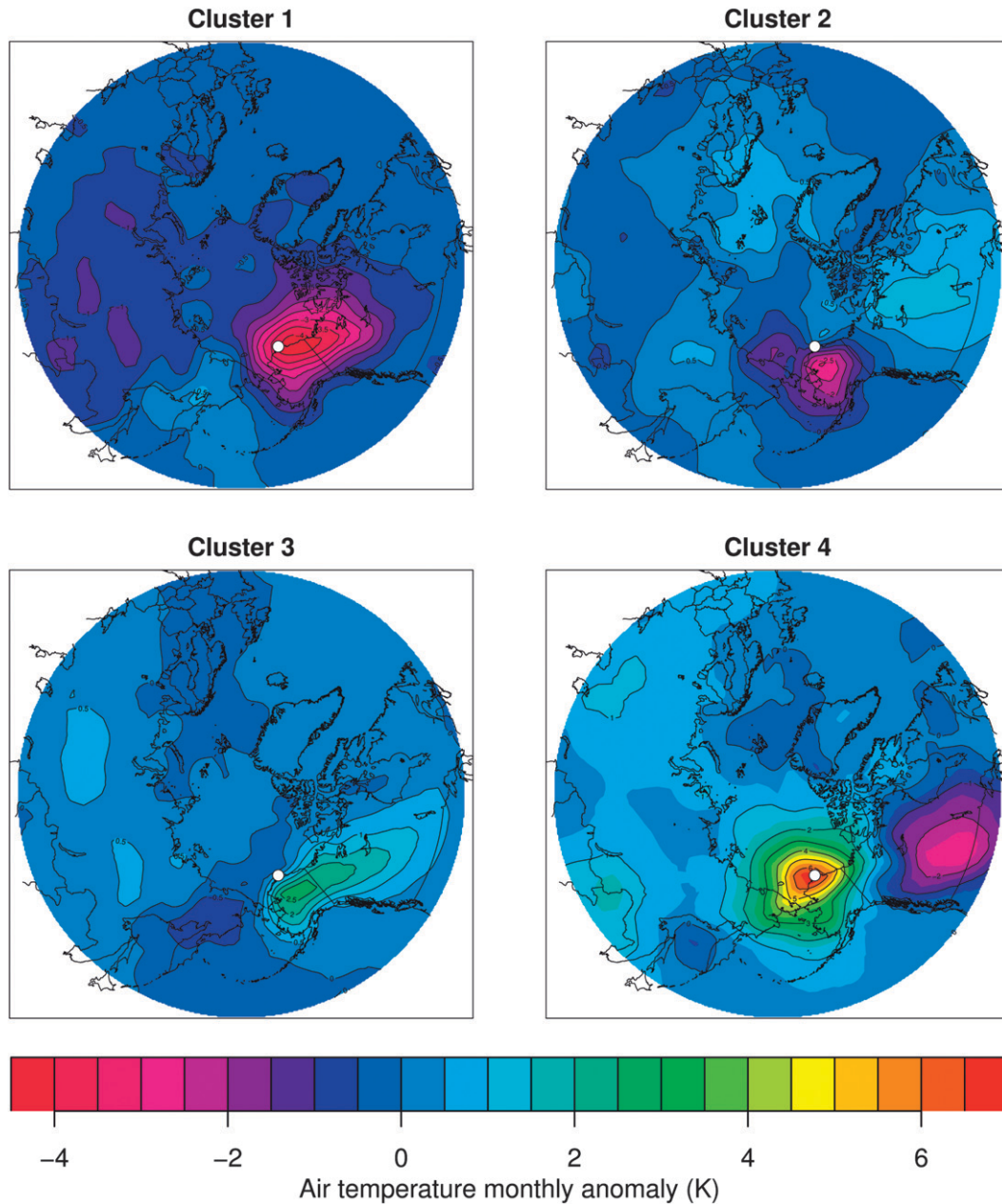


FIG. 7. NCEP–NCAR reanalysis 1 air temperature monthly anomalies at $\sigma = 0.995$, composited for each local meteorological category. Barrow is indicated by the white circle. In cluster 1, cold air from the Arctic Ocean and Beaufort Sea has been advected to northern Alaska. Cluster 2 is also cold, but the source region is the Chukchi Sea. Warm air dominates cluster 3, while cluster 4 is characterized by very high temperature anomaly over northern Alaska and the Chukchi Sea due to advection through the Bering Strait. The temperature anomaly is calculated relative to the 11-yr mean temperature for each calendar month.

conditions, while cluster 3 is occasionally under the influence of high pressure and thus clearer sky. The progression of PWV anomaly can be explained by the origin of the advected air in each cluster, with clusters 3 and 4 having a greater moist and southerly contribution. Similarly, the DLW anomaly reflects the lowering of

cloud-base height and increasing optical thickness of the cloud structures found in increasingly moist advection combined with the higher temperature anomaly of the warmer southerly air masses.

Good discrimination between clusters is seen in many of the cloud-property variables. Discrimination

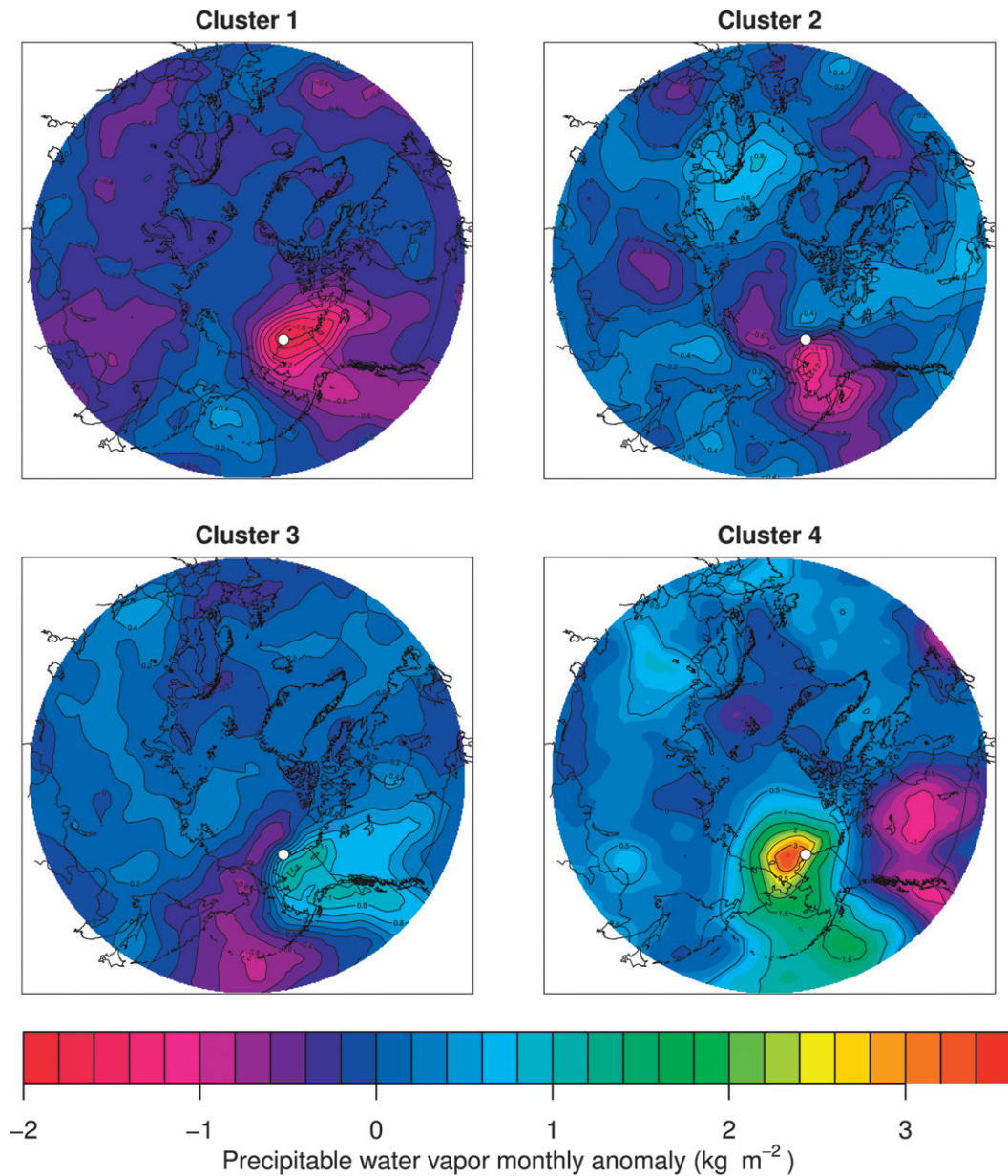


FIG. 8. NCEP–NCAR reanalysis 1 precipitable water vapor monthly anomalies, composited for each local meteorological category. Barrow is indicated by the white circle. The cold air over Barrow in clusters 1 and 2 is dry. In cluster 3, Barrow lies at the boundary between a moist air mass advected from the south and drier air over the Arctic Ocean. Cluster 4, in which Barrow is under the influence of advection through the Bering Strait, exhibits very moist air. The precipitable water vapor anomaly is calculated relative to the 11-yr mean precipitable water vapor for each calendar month.

is assessed between each pair of clusters by performing a two-sample, two-sided Kolmogorov–Smirnov (KS) test (Conover 1980) for each cloud or radiative variable listed in the previous paragraph. This is an unbinned, nonparametric test that quantifies the probability that two samples were drawn from the same parent distribution, and takes into account both differences in the

position and the shape of the distributions. While there are many ways of testing for the similarity of distributions, the KS test is sensitive to both mean and shape of the distributions and at the same time does not require a subjective choice of binning. The KS test takes differences in shape into consideration, so additional subdivision of the distributions by season is not required.

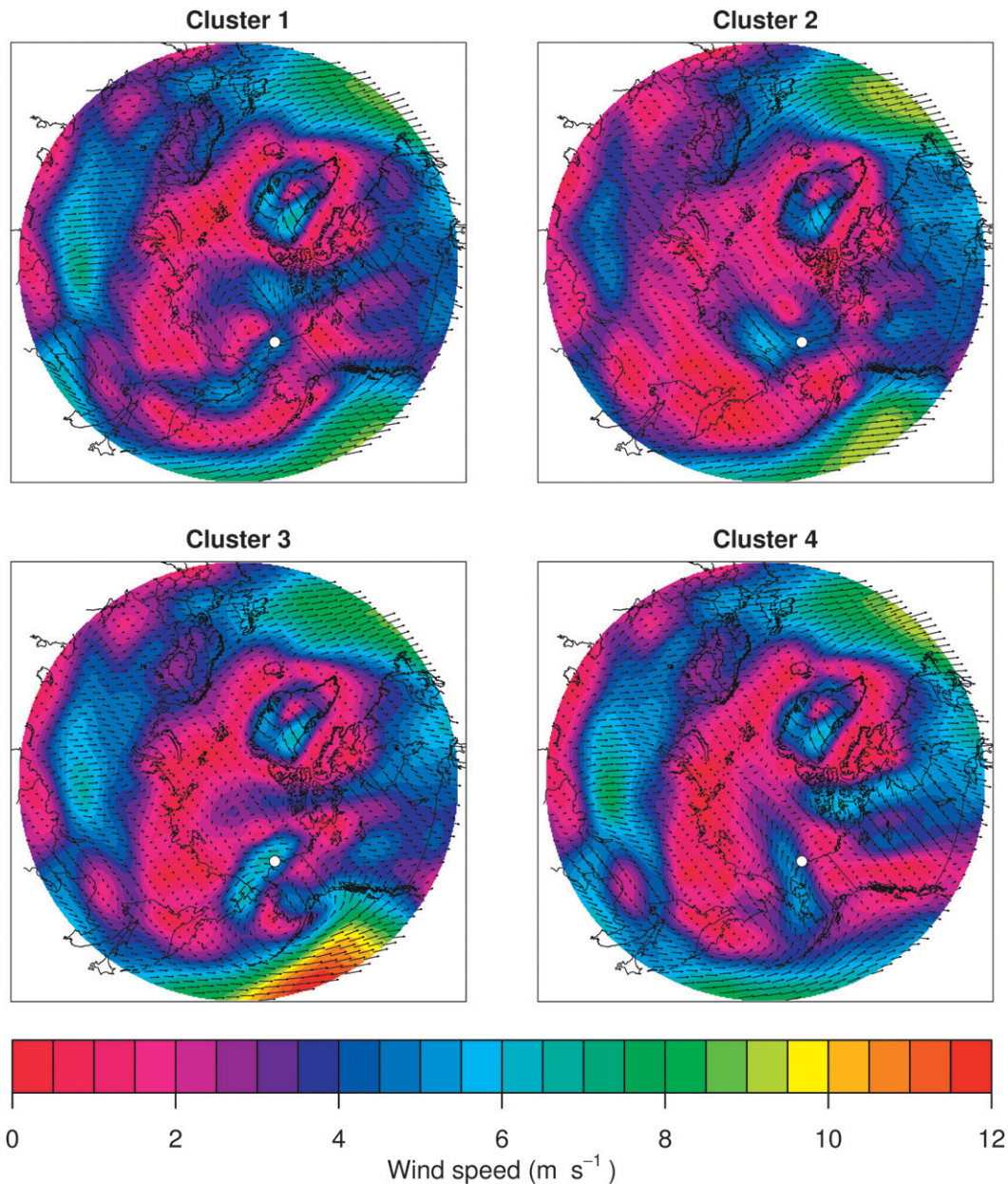


FIG. 9. NCEP–NCAR reanalysis 1 wind speed and direction at 850 hPa, composited for each local meteorological category. Barrow is indicated by the white circle. The color contours show wind speed; arrows show speed (proportional to length) and direction. The anticyclonic flow from the Arctic Ocean and Beaufort Sea over Barrow can be seen clearly in cluster 1, and opposite cyclonic flow from the Chukchi Sea in cluster 2. The strongest winds occur in cluster 3, where Barrow is under the influence of easterly to southeasterly flow at the midlevels of moist air from the Gulf of Alaska. Cluster 4 features moderate-strength winds throughout the Bering Sea and Bering Strait advecting warm, moist air to Barrow.

If the KS test returns agreement with $p < 10^{-5}$, the distributions are considered significantly different. For example, the TSI total-cloud sky cover distributions (shown in Fig. 10) differ significantly between cluster 1 and all other clusters, but the total-cloud sky covers in clusters 2, 3, and 4 are not significantly different from each

other. As another example, the downwelling longwave radiation anomalies (shown in Fig. 11) differ significantly between all clusters.

A list of dissimilar variables is given for each pair of clusters in Table 5. Most clusters differ in many of the cloud variables we have considered, and some

TABLE 4. Summary of cloud and radiative properties of the meteorological categories.

Cluster	Column-integrated and surface-level properties	Cloud-profile properties
1	Lowest downwelling longwave flux anomaly. Clearest skies. Lowest precipitable water vapor path. Small liquid and ice water path except in fall.	Smallest cloud thickness per season. Predominantly ice clouds in winter; shared between ice and mixed-phase cloud near the surface in spring, liquid and mixed phase in summer, and mixed phase in fall.
2	Slightly negative downwelling longwave flux anomaly. Low cloud bases, occasionally midlevel bases. Broken or overcast sky. Below-average precipitable water vapor. High liquid water path (except small in winter), high ice water path.	Thickest low-level cloud in spring, sharp dropoff in midlevels. Predominantly ice clouds in winter; shared between ice and mixed-phase cloud near the surface in spring, liquid and mixed phase in summer, and mixed phase in fall.
3	Slightly positive downwelling longwave flux anomaly. Low cloud bases, occasionally high-level bases or clear sky. Broken or overcast sky, occasionally clear sky. Above-average precipitable water vapor. High liquid water path (except moderate in winter), high ice water path.	Thick cloud throughout column. Ice clouds at the surface in winter, overlaid by mixed phase in the midlevels; mixed phase in spring, liquid overlaid by mixed phase in summer, and mixed phase in fall.
4	Highest downwelling longwave flux anomaly. Low cloud bases, occasionally midlevel bases. Broken or overcast sky. Highest precipitable water vapor. High liquid water path all seasons, high ice-water path in winter and spring, moderate in summer and fall.	Thick cloud throughout column. Mixed-phase cloud in winter and spring, liquid overlaid by mixed phase in summer, and mixed phase in fall.

clusters differ in all cloud variables. Thus we conclude that the surface-meteorology-based clustering can identify characteristic features in cloud properties. For comparison, Table 6 lists the dissimilarities between synoptic categories—it is apparent that clustering based on the local meteorology better distinguishes differing cloud property states than does the synoptic meteorology.

Vertical cloud structure is estimated through profiles of mean cloud-layer thickness, LWC, IWC, and mixed-phase cloud fraction. We calculate daily averages of the ARSCL layer thicknesses in vertical bins (with a bin size of 10 m) as follows: for every ARSCL retrieval, if a bin is in a cloud layer, we increment the bin by the thickness of that layer; we then divide by the number of retrievals available for that day. LWC and IWC profiles are derived from the Microbase product with minimal processing. Daily averages are computed, and the daily-average profiles are interpolated to a uniform vertical layer spacing to account for changes in the radar configuration. [The Microbase column starts at 75 m AGL (2008 and later) or 105 m AGL (2002–08), with a vertical spacing of approximately 45 m.] We also determine the probability of occurrence of mixed-phase cloud conditional on the presence of cloud of any type. MPC is considered to have occurred at a given height if both LWC and IWC are above a minimum threshold (10^{-7} g m⁻³ for ice and 10^{-4} g m⁻³ for water). This threshold is chosen to

eliminate small nonzero signals that are likely noise. If the retrieval contains neither liquid water nor ice, that retrieval is not counted in the denominator when calculating the probability of occurrence. Figure 12 shows the resulting profiles, composited separately for each cluster and season. A sensitivity study was conducted in which the less abundant species was required to be at least a certain threshold fraction of the total (ice + liquid) water content. This threshold was applied in addition to the minimum requirements on ice and liquid water content for a retrieval to be considered cloud. For thresholds 5% and below, there is little change to the MPC profiles. For 10% and above, the differences among the profiles are similar but the amplitude of the MPC probability decreases, especially near the surface.

The observed vertical cloud structures are well explained by the synoptic meteorology described in section 3. Cluster 1, the driest cluster, has the lowest cloud occurrence and lowest mean layer thickness in all seasons. The mean cloud thickness of this cluster is usually less than half that of the other clusters in the lower and middle levels (below 6-km altitude). The only seasonal feature in cluster 1 is the presence of low-level cloud in autumn, consistent with advection from the Arctic Ocean and Beaufort Sea, which have open surface water in autumn. Cluster 4, the moistest, also shows very little seasonal variability in vertical extent or amplitude. In all seasons except autumn, this is the regime

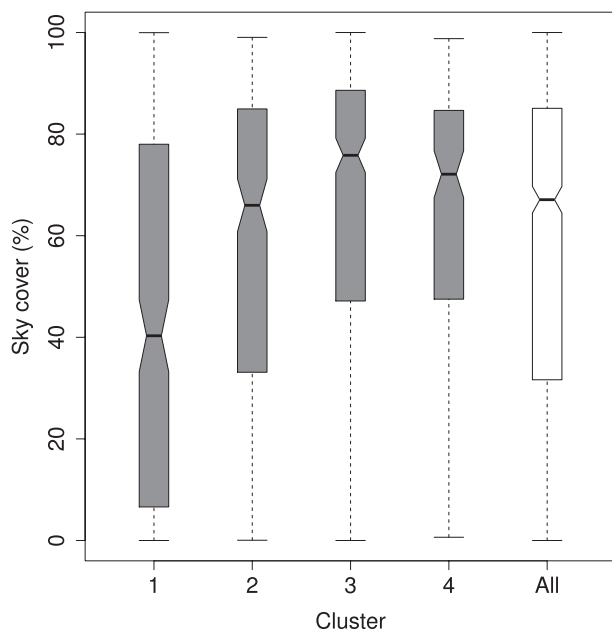


FIG. 10. Distribution resolved by cluster of the TSI total-cloud sky cover (sum of thin and opaque cloud sky cover). The sky-cover distributions differ significantly between cluster 1 and all other clusters, but the distributions in clusters 2, 3, and 4 are not significantly different from each other, according to the two-sided two-sample Kolmogorov–Smirnov test described in the text. Figure 3 explains the features of the box plot.

with the most vertically developed cloud structures, consistent with moist southerly advection in cyclonic flow. (In autumn and winter, the cyclonic flow in cluster 3 is strong enough to advect high- and midlevel clouds from the Gulf of Alaska that are as thick as or thicker than in cluster 4.) In summer, cluster 4 features the thickest clouds throughout the column, presumably because the Bering Strait is already ice-free then, resulting in advection of water vapor at all levels. Cluster 2, which is characterized by cyclonic flow but with low-moisture northwesterly advection from over the Arctic Ocean and Siberian and Chukchi Sea, has the thickest low-level clouds in all seasons except summer but also has the sharpest dropoff in cloudiness at midlevels. Considering the source region, it is not expected that these low pressure systems would contain enough moisture to allow more extensive vertical development. Cluster 3, which is mostly cyclonic flow with advection of moisture from the south, resembles cluster 4 in the presence of thick cloud throughout the column. It differs from cluster 4 in autumn, when the easterly fetch over the open Beaufort Sea (which, unlike the southerly flow over the open Bering Strait in cluster 4, is not disrupted at low levels by orographic barriers before reaching Barrow) leads to low-level cloud layers almost twice as thick as in cluster 4.

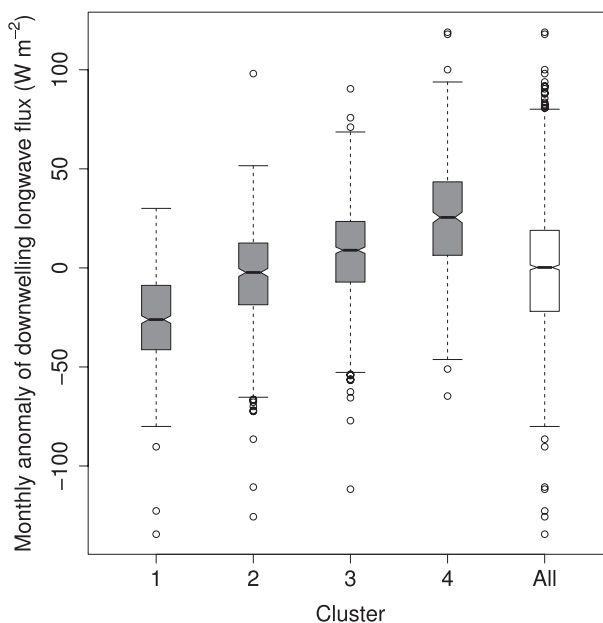


FIG. 11. Distribution resolved by cluster of the SKYRAD downwelling longwave flux monthly anomaly. The distributions differ significantly between all clusters according to the two-sided two-sample Kolmogorov–Smirnov test described in the text. Figure 3 explains the features of the box plot.

Likewise, the thermodynamic-phase structure of the cloud varies strongly between clusters and is explained by the properties of the clusters. In all seasons and clusters, liquid water is predominantly found below about 2-km height. In winter, there are negligible amounts of liquid water in the dry clusters, while the Aleutian-influenced cluster 4 maintains almost half of its summer maximum LWC near the surface. Clusters 1 and 2 are less than 10% water at all levels, with the very dry cluster 1 having lower ice content than cluster 2 throughout the column. Cluster 3 is similar to cluster 2 in ice content, but the maritime influence can be seen in its column-maximum liquid water fraction, which reaches a value 4 times as high as that of cluster 2. Further, the LWC in cluster 3 becomes comparable to cluster 4 at the midlevels in all seasons. Cluster 4, although containing predominantly water below 3 km, still contains more than three times as much ice as the next-highest clusters in the low levels and remains icier throughout the column. Not surprisingly, the two colder clusters rarely feature mixed-phase cloud at any height in winter, while for the warmer clusters MPC is the dominant cloud type at least at some heights (between the surface and 3 km for cluster 4, and between 1 and 3 km for cluster 3). In the spring, the liquid water content of all clusters rises, though only modestly for the already wet cluster 4. Near the surface, there is little difference in LWC between

TABLE 5. Table of significant differences in cloud properties between surface meteorology categories. For each pair of categories, we list the cloud properties whose distributions are significantly dissimilar. The metric for dissimilarity is $p < 10^{-5}$ in a two-sided, two-sample Kolmogorov–Smirnov test. Cloud properties considered are clear (C), midlevel (M; 2000–4000 m AGL), and low (L; 0–2000 m AGL) cloud bases; cloud fraction; monthly anomaly of precipitable water vapor (PWV) and liquid water path (LWP); monthly anomaly of downwelling longwave radiation (DLW); and number concentration of condensation nuclei (CN). The sources of these measurements are described in the text.

Cluster	1	2	3	4
1		Cloud base (C, M, L) Cloud cover PWV, LWP, IWP DLW CN	Cloud base (C, L) Cloud cover PWV, LWP, IWP DLW	Cloud base (C, M, L) Cloud cover PWV, LWP, IWP DLW CN
2	Cloud base (C, M, L) Cloud cover PWV, LWP, IWP DLW CN		Cloud base (M) PWV DLW CN	PWV, LWP DLW
3	Cloud base (C, L) Cloud cover PWV, LWP, IWP DLW	Cloud base (M) PWV DLW CN		Cloud base (M, L) PWV, LWP DLW CN
4	Cloud base (C, M, L) Cloud cover PWV, LWP, IWP DLW CN	PWV, LWP DLW	Cloud base (M, L) PWV, LWP DLW CN	

any clusters except the driest (cluster 1), whose LWC is about half as large. The two Arctic Ocean–influenced clusters resemble each other closely in the prevalence of MPC, which is about half near the surface and tapers to all ice at 4 km height. The same is true for the Pacific Ocean–influenced clusters, which are 80% MPC below 3 km. This picture is reversed in summer, when the warmer clusters are almost ice free near the surface, while 50% of the clouds in the colder clusters are still mixed phase. This fraction rises to >80% for all clusters in the midlevels, where all clusters have their IWC column maximum. Cluster 1 continues to be the driest, with a LWC one-third as large as that of the other clusters near the surface. In the fall, all clusters bring large amounts of

liquid and ice water to the layers just above the surface, presumably from local evaporation off the open ocean. These clouds are predominantly mixed phase for all clusters. Above the low-level cloud layer, the colder clusters quickly become all ice, while the Pacific-influenced clusters remain mixed phase to about 4-km height.

5. Constructing test cases for model evaluation

As we have seen above, the cloud properties differ significantly between clusters. This variation in cloud properties between clusters means that each cluster exposes the models to different potential sources of failure. At the same time, the variation is not a simple

TABLE 6. Table of significant differences in cloud properties between synoptic meteorology categories. For each pair of categories, we list the cloud properties whose distributions are significantly dissimilar. The metric for dissimilarity is $p < 10^{-5}$ in a two-sided, two-sample Kolmogorov–Smirnov test. Cloud properties considered are the same as in Table 5. Synoptic categories are abbreviated as in Table 3. Category pairs that do not differ significantly in any cloud property are marked with a dash.

Synoptic	AOL	SL	ABL	AOH	SH	ABH
AOL		PWV	—	—	—	—
SL	PWV		—	Cloud base (M); PWV; CN	PWV; CN	—
ABL	—	—		Cloud base (M)	PWV; CN	—
AOH	—	Cloud base (M); PWV; CN	Cloud base (M)		—	—
SH	—	PWV; CN	PWV; CN	—		—
ABH	—	—	—	—	—	

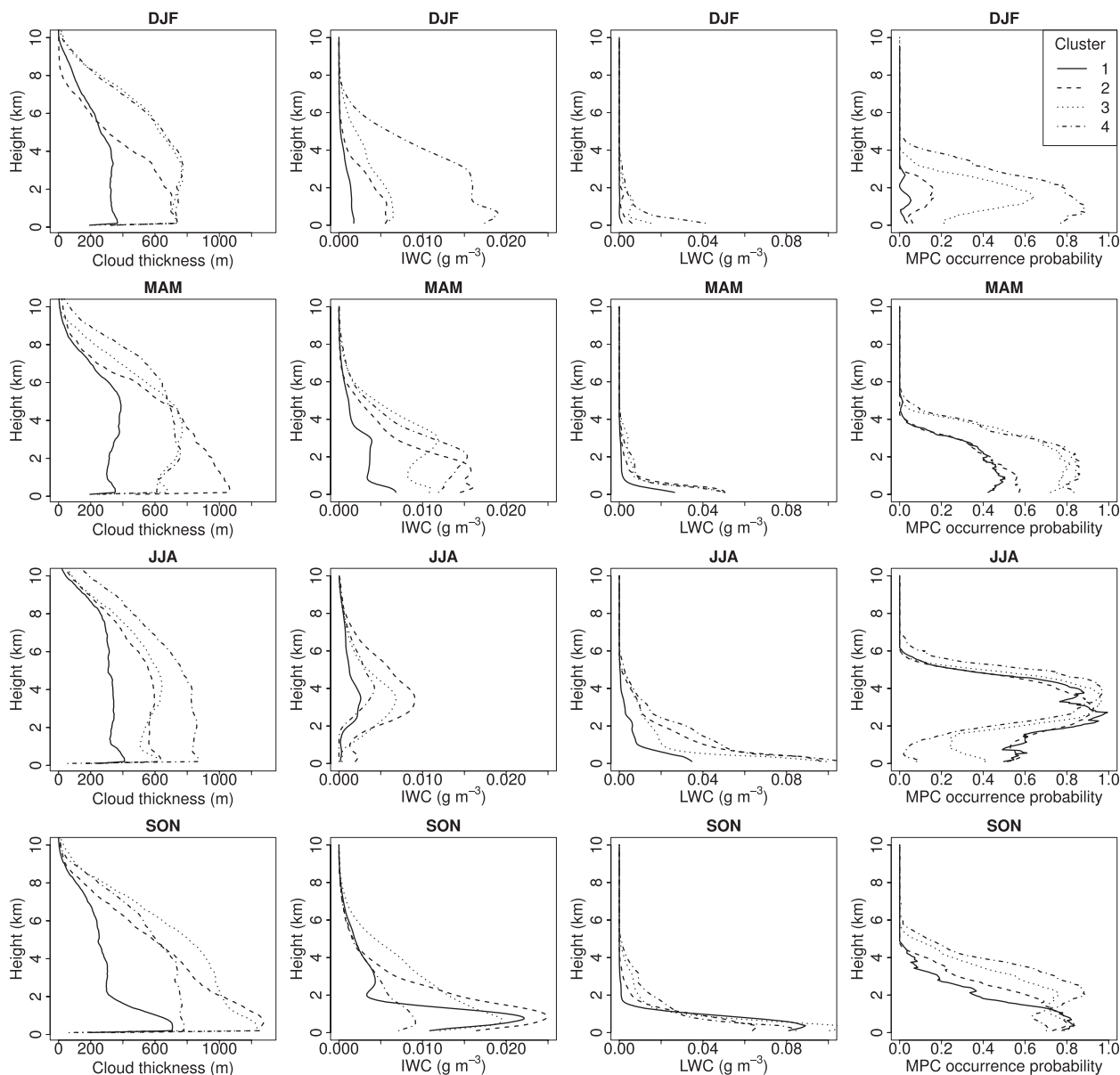


FIG. 12. Vertical profiles of average cloud thickness, ice water content (IWC), liquid water content (LWC), and probability of occurrence of mixed-phase cloud (MPC). All profiles are separately composited by season (rows) and meteorological regime (line style). Cloud thickness is reconstructed from ARSCL. The remaining quantities are reconstructed from Microbase. The presence of mixed-phase cloud is estimated by testing for simultaneous nonzero LWC and IWC at the same height, and is conditional upon the presence of cloud of any kind.

slicing in each of the cloud-property variables; instead, the conditions are grouped into meteorologically meaningful categories. The multidimensional phase space of physically significant cloud variables is reduced to a discrete space of k clusters (in our case 4).

Comparing model output and observations separately for each category is beneficial by steering a course between two adverse conditions: an artificially narrow range of conditions that would result from cloud-variable

slicing versus the overwhelming number of test cases that would result from performing model comparisons for each day in the time series without some form of categorization. From a statistical standpoint, the cluster-based model evaluation technique confers another benefit: it provides plenty of statistics in each test case, which tends to make the results more robust against random fluctuations. In the time series data used in this paper, there are between 587 and 1068 days available

for comparison in each of the categories, a vast increase over the $O(10)$ days usually found in field campaigns. Modelers can use this classification method by retrieving the list identifying the category for each day used in this study (available online at <http://aerosol.ucsd.edu/supplement/arm-nsa-met>).

6. Summary and conclusions

In response to the large model uncertainties of clouds in the Arctic, it is desirable to use long time series of cloud-property observations in studies that test models. We have developed a method that assembles long time series of meteorological observations into test cases for model evaluation. The method uses an objective clustering algorithm to sort the observations into subsets of meteorologically similar conditions. We have applied this method to standard surface-meteorological observations (surface pressure, air temperature, relative humidity, and horizontal wind components) collected between 1 January 2000 and 31 December 2010 at the NSA site of the DOE ARM Program. Four categories with distinct combinations of meteorological properties emerge. Cluster 1 is cold, dry, and with high pressure. Cluster 2 is slightly below mean temperature and dry. Cluster 3 is low pressure, humid, and slightly above mean temperature, with high winds from the east or northeast. Cluster 4 is very warm and moist with close to mean surface pressure.

These categories were shown to correlate with synoptic meteorological regimes influencing the NSA site that were identified in NCEP reanalysis fields. These synoptic regimes include well-known features such as the Aleutian low and the Beaufort Sea high. In cluster 1, high pressure over the Arctic Ocean and the Beaufort Sea dominates, with cold, dry anticyclonic flow from the north explaining the observed conditions. Cluster 2 is influenced by low pressure to the north of Barrow, with cyclonic flow that nevertheless is fairly dry because of its polar origin. In cluster 3, strong cyclonic flow over the Gulf of Alaska transports moist air over the Alaskan peninsula in the mid and high levels (above the Alaskan coastal ranges), while the lower levels are also under the influence of weak high pressure over the Beaufort Sea. Cluster 4 advects very warm, moist air through the Bering Strait in cyclonic flow around Aleutian low pressure systems.

Further, we showed that the distinct meteorological regimes bring with them distinct cloud properties. These cloud structures are well explained by the synoptic regimes associated with the categories. Cluster 1 is fairly dry at all levels, consistent with anticyclonic polar flow. Only during fall are there thick clouds near the surface, presumably from local evaporation over

the Beaufort Sea. During the cold seasons, whatever clouds exist in cluster 1 predominantly contain ice, and during the warm season they are frequently mixed phase. Cluster 2 is moister than cluster 1, frequently with thick clouds especially in the lower levels, but with similar seasonal thermodynamic-phase behavior. The clouds extend into the higher troposphere more frequently in clusters 3 and 4 than in clusters 1 and 2, consistent with moist cyclonic flow from the south. Mixed-phase cloud for clusters 3 and 4 extends to about 5-km height in the summer and 3 km in the winter, with relatively rare probability of occurrence near the surface in the summer. In all seasons except fall, cluster 4 has the greatest column-integrated water content; in fall, moist low-level clouds of local origin occur in cluster 3.

The observations collected at the ARM NSA site are ideally suited for cloud modeling studies because of the high quality of the comprehensive cloud-variable dataset. The classification presented here, which is the first time that a long time series of Arctic cloud observations has been assembled into meteorologically similar regimes, is offered as a potentially useful complement to model–observation comparison studies based on field campaign data. The observations in each category span the variation of conditions expected within each meteorological regime, so that comparing model output and observations separately for each category exposes models to the range of conditions found in long time series data. At the same time, the overwhelming phase space of physically significant variables is assembled into a small number of meteorologically meaningful categories. This suggests that the categories produced by the method are useful as model-evaluation test cases, which is the subject of ongoing research.

Acknowledgments. This work was funded by the Department of Energy under Contracts DE-SC0001962 and DE-AC02-98CH10886 and the Earth System Modeling Program via the FASTER Project. We thank Mike Jensen for informative discussions about Microbase. The computational resources required for this work were accessed via the GlideinWMS (Siligoi et al. 2009) on the Open Science Grid (Pordes et al. 2008). Data were obtained from: the Atmospheric Radiation Measurement (ARM) Program sponsored by the U.S. Department of Energy, Office of Science, Office of Biological and Environmental Research, Climate and Environmental Sciences Division; the National Oceanic and Atmospheric Administration (NOAA) Climate Monitoring and Diagnostics Laboratory (CMDL) Aerosols Group; and the NOAA Office of Oceanic and Atmospheric Research (OAR) Earth System Research Library (ESRL) Physical Science Division (PSD).

REFERENCES

- Ackerman, T. P., and G. M. Stokes, 2003: The Atmospheric Radiation Measurement program. *Phys. Today*, **56**, 38–44, doi:10.1063/1.1554135.
- Barber, D. G., and J. M. Hanesiak, 2004: Meteorological forcing of sea ice concentrations in the southern Beaufort Sea over the period 1979 to 2000. *J. Geophys. Res.*, **109**, C06014, doi:10.1029/2003JC002027.
- Bodhaine, B. A., 1989: Barrow surface aerosol: 1976–1986. *Atmos. Environ.*, **23**, 2357–2369.
- Briegleb, B. P., and D. H. Bromwich, 1998: Polar climate simulation of the NCAR CCM3. *J. Climate*, **11**, 1270–1286.
- Clothiaux, E. E., T. P. Ackerman, G. G. Mace, K. P. Moran, R. T. Marchand, M. A. Miller, and B. E. Martner, 2000: Objective determination of cloud heights and radar reflectivities using a combination of active remote sensors at the ARM CART sites. *J. Appl. Meteor.*, **39**, 645–665.
- Conover, W. J., 1980: *Practical Nonparametric Statistics*. 2nd ed. John Wiley and Sons, 493 pp.
- Curry, J. A., and G. F. Herman, 1985: Relationships between large-scale heat and moisture budgets and the occurrence of Arctic stratus clouds. *Mon. Wea. Rev.*, **113**, 1441–1457.
- , and E. E. Ebert, 1992: Annual cycle of radiation fluxes over the Arctic Ocean: Sensitivity to cloud optical properties. *J. Climate*, **5**, 1267–1280.
- , W. B. Rossow, D. Randall, and J. L. Schramm, 1996: Overview of Arctic cloud and radiation characteristics. *J. Climate*, **9**, 1731–1764.
- , and Coauthors, 2000: FIRE Arctic Clouds Experiment. *Bull. Amer. Meteor. Soc.*, **81**, 5–29.
- Fowler, L. D., D. A. Randall, and S. A. Rutledge, 1996: Liquid and ice cloud microphysics in the CSU general circulation model. Part 1: Model description and simulated microphysical processes. *J. Climate*, **9**, 489–529.
- Fridlind, A. M., A. S. Ackerman, G. McFarquhar, G. Zhang, M. R. Poellot, P. J. DeMott, A. J. Prenni, and A. J. Heymsfield, 2007: Ice properties of single-layer stratocumulus during the Mixed-Phase Arctic Cloud Experiment: 2. Model results. *J. Geophys. Res.*, **112**, D24202, doi:10.1029/2007JD008646.
- Gordon, N. D., J. R. Norris, C. P. Weaver, and S. A. Klein, 2005: Cluster analysis of cloud regimes and characteristic dynamics of midlatitude synoptic systems in observations and a model. *J. Geophys. Res.*, **110**, D15S17, doi:10.1029/2004JD005027.
- Hartigan, J. A., 1975: *Clustering Algorithms*. John Wiley and Sons, 351 pp.
- , and M. A. Wong, 1979: Algorithm AS 136: A *k*-means clustering algorithm. *J. Roy. Stat. Soc.*, **28C**, 100–108.
- Inoue, J., J. Liu, J. O. Pinto, and J. A. Curry, 2006: Intercomparison of Arctic regional climate models: Modeling clouds and radiation for SHEBA in May 1998. *J. Climate*, **19**, 4167–4178.
- Jakob, C., and G. Tselioudis, 2003: Objective identification of cloud regimes in the tropical western Pacific. *Geophys. Res. Lett.*, **30**, 2082, doi:10.1029/2003GL018367.
- Jayaweera, K., 1982: Meteorological conditions conducive to the formation of stratus clouds over the Beaufort Sea. *Climatology*, **7**, 25–32.
- Kalnay, E., and Coauthors, 1996: The NCEP/NCAR 40-Year Reanalysis Project. *Bull. Amer. Meteor. Soc.*, **77**, 437–471.
- Kay, J. E., and A. Gettelman, 2009: Cloud influence on and response to seasonal Arctic sea ice loss. *J. Geophys. Res.*, **114**, D18204, doi:10.1029/2009JD011773.
- Klein, S. A., and Coauthors, 2009: Intercomparison of model simulations of mixed-phase clouds observed during the ARM Mixed-Phase Arctic Cloud Experiment. I: Single-layer cloud. *Quart. J. Roy. Meteor. Soc.*, **135**, 979–1002, doi:10.1002/qj.416.
- MacQueen, J., 1967: Some methods for classification and analysis of multivariate observations. *Proceedings of the Fifth Berkeley Symposium on Mathematical Statistics and Probability*, Vol. 1, L. M. Le Cam and J. Neyman, Eds., University of California Press, 281–297.
- Marchand, R., N. Beagley, and T. P. Ackerman, 2009: Evaluation of hydrometeor occurrence profiles in the multiscale modeling framework climate model using atmospheric classification. *J. Climate*, **22**, 4557–4573.
- Maslanik, J. A., M. C. Serreze, and R. G. Barry, 1996: Recent decreases in Arctic summer ice cover and linkages to atmospheric circulation anomalies. *Geophys. Res. Lett.*, **23**, 1677–1680.
- Maxwell, J. B., 1981: Climatic regions of the Canadian Arctic islands. *Arctic*, **34**, 225–240.
- McFarquhar, G. M., and Coauthors, 2011: Indirect and Semi-Direct Aerosol Campaign: The impact of Arctic aerosols on clouds. *Bull. Amer. Meteor. Soc.*, **92**, 183–201.
- McGill, R., J. W. Tukey, and W. A. Larsen, 1978: Variations of box plots. *Amer. Stat.*, **32**, 12–16.
- Meyers, M. P., R. L. Walko, J. Y. Harrington, and W. R. Cotton, 1997: New RAMS cloud microphysics parameterization. Part II: The two-moment scheme. *Atmos. Res.*, **45**, 3–39.
- Milbrandt, J. A., and M. K. Yau, 2005: A multimoment bulk microphysics parameterization. Part I: Analysis of the role of the spectral shape parameter. *J. Atmos. Sci.*, **62**, 3051–3064.
- Morrison, H., and J. O. Pinto, 2005: Mesoscale modeling of springtime Arctic mixed-phase stratiform clouds using a new two-moment bulk microphysics scheme. *J. Atmos. Sci.*, **62**, 3683–3704.
- , and A. Gettelman, 2008: A new two-moment bulk stratiform cloud microphysics scheme in the Community Atmosphere Model, version 3 (CAM3). Part I: Description and numerical tests. *J. Climate*, **21**, 3642–3659.
- , and W. W. Grabowski, 2008: A novel approach for representing ice microphysics in models: Description and tests using a kinematic framework. *J. Atmos. Sci.*, **65**, 1528–1548.
- , and Coauthors, 2009: Intercomparison of model simulations of mixed-phase clouds observed during the ARM Mixed-Phase Arctic Cloud Experiment. II: Multilayer cloud. *Quart. J. Roy. Meteor. Soc.*, **135**, 1003–1019.
- , G. de Boer, G. Feingold, J. Harrington, M. D. Shupe, and K. Sulia, 2012: Resilience of persistent Arctic mixed-phase clouds. *Nat. Geosci.*, **5**, 11–17.
- Overland, J. E., 2009: Meteorology of the Beaufort Sea. *J. Geophys. Res.*, **114**, C00A07, doi:10.1029/2008JC004861.
- Parkinson, C. L., 1990: The impact of the Siberian high and Aleutian low on the sea-ice cover of the Sea of Okhotsk. *Ann. Glaciol.*, **14**, 226–229.
- Pordes, R., and Coauthors, 2008: New science on the Open Science Grid. *J. Phys.*, **125**, 012070, doi:10.1088/1742-6596/125/1/012070.
- Proshutinsky, A. Y., and M. A. Johnson, 1997: Two circulation regimes of the wind driven Arctic Ocean. *J. Geophys. Res.*, **102** (C6), 12 493–12 514.
- Przybylak, R., 2003: *The Climate of the Arctic*. 1st ed. Kluwer Academic, 288 pp.
- Reed, R. J., and B. A. Kunkel, 1960: The Arctic circulation in summer. *J. Meteor.*, **17**, 489–506.
- Rogers, J. C., 1978: Meteorological factors affecting interannual variability of summertime ice extent in Beaufort Sea. *Mon. Wea. Rev.*, **106**, 890–897.

- Rotstain, L. D., B. F. Ryan, and J. J. Katzfey, 2000: A scheme for calculation of the liquid fraction in mixed-phase stratiform clouds in large-scale models. *Mon. Wea. Rev.*, **128**, 1070–1088.
- Sandvik, A., M. Biryulina, N. G. Kvamsto, J. J. Stamnes, and K. Stamnes, 2007: Observed and simulated microphysical composition of Arctic clouds: Data properties and model validation. *J. Geophys. Res.*, **112**, D05205, doi:10.1029/2006JD007351.
- Serreze, M. C., and R. G. Barry, 2005: *The Arctic Climate System*. Cambridge University Press, 385 pp.
- , J. E. Box, R. G. Barry, and J. E. Walsh, 1993: Characteristics of Arctic synoptic activity, 1952–1989. *Meteor. Atmos. Phys.*, **51**, 147–164.
- Sfiligoi, I., D. C. Bradley, B. Holzman, P. Mhashilkar, S. Padhi, and F. Würthwein, 2009: The pilot way to grid resources using glideinWMS. *Proc. 2009 WRI World Congress on Computer Science and Information Engineering*, Los Angeles, CA, CSIE, 428–432.
- Shupe, M. D., 2011: Clouds at Arctic atmospheric observatories. Part II: Thermodynamic phase characteristics. *J. Appl. Meteor. Climatol.*, **50**, 645–661.
- , and J. M. Intrieri, 2004: Cloud radiative forcing of the Arctic surface: The influence of cloud properties, surface albedo, and solar zenith angle. *J. Climate*, **17**, 616–628.
- , S. Y. Matrosov, and T. Uttal, 2006: Arctic mixed-phase cloud properties derived from surface-based sensors at SHEBA. *J. Atmos. Sci.*, **63**, 697–711.
- Solomon, A., H. Morrison, O. Persson, M. D. Shupe, and J.-W. Bao, 2009: Investigation of microphysical parameterizations of snow and ice in Arctic clouds during M-PACE through model–observation comparisons. *Mon. Wea. Rev.*, **137**, 3110–3128.
- Stamnes, K., B. Zak, and G. E. Shaw, 1995: The Atmospheric Radiation Measurements (ARM) Program—ARM’s window on the Arctic. *Sci. Total Environ.*, **160–61**, 825–829.
- , R. G. Ellingson, J. A. Curry, J. E. Walsh, and B. D. Zak, 1999: Review of science issues, deployment strategy, and status for the ARM North Slope of Alaska–Adjacent Arctic Ocean climate research site. *J. Climate*, **12**, 46–63.
- Stone, R. S., 1997: Variations in western Arctic temperatures in response to cloud radiative and synoptic-scale influences. *J. Geophys. Res.*, **102** (D18), 21 769–21 776.
- Thompson, G., R. M. Rasmussen, and K. Manning, 2004: Explicit forecasts of winter precipitation using an improved bulk microphysics scheme. Part I: Description and sensitivity analysis. *Mon. Wea. Rev.*, **132**, 519–542.
- , P. R. Field, R. M. Rasmussen, and W. D. Hall, 2008: Explicit forecasts of winter precipitation using an improved bulk microphysics scheme. Part II: Implementation of a new snow parameterization. *Mon. Wea. Rev.*, **136**, 5095–5115.
- Tsay, S.-C., and K. Jayaweera, 1984: Physical characteristics of Arctic stratus clouds. *J. Climate Appl. Meteor.*, **23**, 584–596.
- Uttal, T., and Coauthors, 2002: Surface heat budget of the Arctic Ocean. *Bull. Amer. Meteor. Soc.*, **83**, 255–275.
- Vavrus, S., 2004: The impact of cloud feedbacks on Arctic climate under greenhouse forcing. *J. Climate*, **17**, 603–615.
- Verlinde, J., and Coauthors, 2007: The Mixed-Phase Arctic Cloud Experiment. *Bull. Amer. Meteor. Soc.*, **88**, 205–221.
- Wang, X., and J. R. Key, 2003: Recent trends in Arctic surface, cloud, and radiation properties from space. *Science*, **299**, 1725–1728.
- , and —, 2005: Arctic surface, cloud, and radiation properties based on the AVHRR Polar Pathfinder dataset. Part I: Spatial and temporal characteristics. *J. Climate*, **18**, 2558–2574.
- Zhao, C., and Coauthors, 2012: Toward understanding of differences in current cloud retrievals of ARM ground-based measurements. *J. Geophys. Res.*, **117**, D10206, doi:10.1029/2011JD016792.